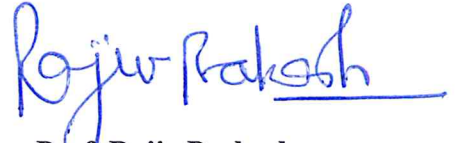


CERTIFICATE

It is certified that the work contained in the thesis titled “**GRAPHITIC CARBON NITRIDE AND CARBON COMPOSITES FOR ELECTRO- AND PHOTOCHEMICAL APPLICATIONS**” by “**ANIRUDDHA JAISWAL**” has been carried out under my supervision and that this work has not been submitted elsewhere for a degree.

It is further certified that the student has fulfilled all the requirements of Comprehensive Examination, Candidacy and SOTA for the award of Ph.D. Degree.

Date: 21/02/2022



Prof. Rajiv Prakash

(Supervisor)

Professor/आचार्य

School of Materials Science & Technology/पदार्थ विज्ञान एवं प्रौद्योगिकी स्कूल
Indian Institute of Technology/भारतीय प्रौद्योगिकी संस्थान
(Banaras Hindu University), Varanasi/काशी हिन्दू विश्वविद्यालय, वाराणसी

DECLARATION BY THE CANDIDATE

I, "ANIRUDDHA JAISWAL", certify that the work embodied in this thesis is my own bonafide work and carried out by me under the supervision of "PROF. RAJIV PRAKASH" from January 2017 to February 2022, at the "SCHOOL OF MATERIALS SCIENCE AND TECHNOLOGY", Indian Institute of Technology (Banaras Hindu University), Varanasi. The matter embodied in this thesis has not been submitted for the award of any degree/diploma. I declare that I have faithfully acknowledged and given credits to the person/researcher/scientist/institute wherever their works have been cited in my work in this thesis. I further declare that I have not willfully copied any other's work, paragraph, text, data, results, image, etc., reported in journals, books, magazines, reports, dissertations, thesis, etc., or available at websites and have not included them in this thesis and have not cited as my own work.

Date: 21/02/2022

Place: Varanasi

Aniruddha
Jaiswal

Signature of the Student

(ANIRUDDHA JAISWAL)

CERTIFICATE BY THE SUPERVISOR

It is certified that the above statement made by the student is correct to the best of my knowledge.

Rajiv Prakash
(Rajiv Prakash) 21/2/2022

Supervisor
Professor/आचार्य

School of Materials Science & Technology/पदार्थ विज्ञान एवं प्रौद्योगिकी स्कूल
Indian Institute of Technology/भारतीय प्रौद्योगिकी संस्थान
(Banaras Hindu University), Varanasi/काशी हिन्दू विश्वविद्यालय, वाराणसी

Chandana Rath
(Chandana Rath) 21/2/2022

Coordinator
Coordinator/समन्वयक

School of Materials Science & Technology/पदार्थ विज्ञान एवं प्रौद्योगिकी स्कूल
Indian Institute of Technology/भारतीय प्रौद्योगिकी संस्थान
(Banaras Hindu University), Varanasi/काशी हिन्दू विश्वविद्यालय, वाराणसी

COPYRIGHT TRANSFER CERTIFICATE

Title of the Thesis: Graphitic Carbon Nitride and Carbon Composites for Electro-
and Photochemical Applications

Name of the Student: ANIRUDDHA JAISWAL

Copyright Transfer

The undersigned hereby assigns to the Indian Institute of Technology (Banaras Hindu University), Varanasi all rights under copyright that may exist in and for the above thesis submitted for the award of the “*Doctor of Philosophy*”.

Date: 21/02/2022

Place: Varanasi



Signature of the Student
(ANIRUDDHA JAISWAL)

Note: However, the author may reproduce or authorize others to reproduce materials extracted verbatim from the thesis or derivative of the thesis for the author's personal use provided that the source and the Institute's copyright notice are indicated.

Acknowledgment

The work compiled in this thesis has come in the present form only with many direct and indirect helping hands, without acknowledging them I cannot proceed. I take this opportunity to acknowledge and extend my deep gratitude to all those people in whose association and assistance, this whole work could be accomplished and came in the present form.

*At this moment of accomplishment, first and foremost, I would like to pay homage to the founder of Banaras Hindu University, **Pandit Madan Mohan Malviyaa Ji**, a visionary educationist, a social reformer, and an outstanding statesman who made this great temple of education to diffuse spiritual, scientific, technical and professional knowledge to the nation and the world.*

*I embrace this moment to express my deep sense of gratitude to my Supervisor and Ph.D. Guide **Prof. Rajiv Prakash**, School of Materials Science and Technology, IIT(B.H.U.), Varanasi for his constant guidance, valuable suggestion, and positive remarks during the interaction and in my whole journey of the Ph.D. His encouragement, intellectual prowess, loving persona, and valuable ideas guided me to easily fare through my research journey and enables me for a deeper understanding of the research subject. His affectionate behavior and solution-focused approach have been a source of inspiration for me. His complete personality and scientific temperament will act as a Renewable source of motivation, guidance, and learning throughout my life.*

*I would like to express my wholehearted gratitude to **Prof. D. Pandey** (Former Director), **Prof. P. Maiti**, **Dr. C. Upadhyaya**, **Dr. B. N. Pal**, **Dr. S. Singh**, **Dr. A. K. Mishra**, **Dr. S. K. Mishra**, and **Dr. Nikhil** (School of Materials Science and Technology), IIT (B.H.U.), Varanasi for all the fruitful discussions, valuable suggestions during my interactions with them. I am thankful to the former coordinator **Dr. A.K. Singh** and present coordinator **Dr. (Mrs.) C. Rath** for ensuring the availability of common instrumental facilities in the school. I would like to express my sincere thanks to my Research Progress Evaluation Committee (RPEC) member **Dr. I. Sinha**, Department of Chemistry, IIT (B.H.U.) for his remarks and suggestions in each evaluation meeting since joining the school.*

*I also owe my gratitude to **Prof. S. R. Singh** and **Prof. J. Kumar** (both visiting faculty of SMST) for the positive discussions during their tenure in the school. I am indebted to **Prof. S. Bhattacharya** (Department of Chemistry, B.H.U.) and **Prof. R. T. Karunakaran**, NIT, Tiruchirappalli for evaluating my annual research progress report as an external member. I also acknowledge **Dr. A. S. K. Sinha**, Former Dean (Academic), during my initial 2 years in the research.*

*I am greatly thankful to the Central Instrument Facility IIT(BHU), its Prof-in-charge Our Guide **Dr. Prakash**, employees, and instruments operators for ensuring the availability and proper functioning of many critical characterization instruments, we needed to successfully carry out our research work. I also owe my positive thanks to the **Council of Scientific and Industrial Research (CSIR)**, New Delhi for the financial assistance in form of two years of the Junior Research Fellowship (JRF) and later three years of Senior Research Fellowship (SRF) to carry out my research work in financial peace and security.*

*The successful completion of my research work will not be possible without acknowledging the many positive support and fruitful discussion of many of my senior lab members and people from my department and work-field since joining the SMST. I deeply acknowledge **Dr. Monika**, **Dr. Gopal**, **Dr. N.R. Nirala**, **Dr. Uday Pratap**, **Dr. Neeraj**, **Dr. Kashish**, **Dr. Preeti**, **Dr. Richa**, **Dr. Vinita**, **Dr. Manish**, and **Dr. Chandrajeet** for their assistance to accomplish this journey. I have special gratitude to **Dr. Ashish Kumar** for guiding me to solve the tricky reviewer's comment and giving the manuscript its final shape. He gave his valuable time and suggestions for shaping my thesis in the present form. He is a nice and thoughtful mentor with a solution-focused attitude.*

*I acknowledge my fellow lab-mates **Vineet**, **Ravi**, **Nikhil**, **Bishnu**, **Ajay**, **Priya**, **Shweta**, **Subhajeet**, **Saurabh**, **Nupur**, **Shipra**, **Rajpal**, **Radhe Shyam**, (PhDs) **Shivam**, **Karthik**, **Radha**, (MTechs) **Avichal**, **Akash** (IDDs) for their helping hands. I am grateful to all the non-teaching staff from my SMST office for their assistance at all levels.*

The Journey to reach this milestone of writing this thesis for the award of the 'Doctorate' degree is really very long with many ups and downs. With the grace of God, I have many friends and colleagues from my past and present institutions

who made the path smooth to me while going through the different phases. I am grateful to my friends **Siddhartha, Vibhanshu, Yogesh, Avinash, Shere Afgan, Nandita, Rajeev Bhaiya**, from B.H.U. and **Murli, Raman, Shyam Babu, Deepti, Jyoti, Anupam** from the present Institute. I also acknowledge to my friends **Sonu yadav, Narendra bhaiya, Girish Ji, Vinay bhai, Shiv bhaiya**, and many unaccounted names I could not mention unknowingly. These are just a few helping hands, there are much more direct and indirect support of individuals who came across in this journey.

I express my deep indebtedness to my mother, guardian, and a strong woman **Smt. Usha Jaiswal**, my father **Late Shri Daya Prasad Jaiswal**, and my only family member-sister **Ms. Anamika Jaiswal** for their unconditional support. I feel very fortunate to be born and grown up in this Benares city and got the opportunity to complete all my academics here. Of course, it's the grace of the Almighty "**Kashi Vishwanath**" and His blessings.

Table of Contents

		Page Number
List of Figures		i-vi
List of Tables		vii
List of Acronyms/Abbreviations		viii-xi
Preface		xii-xiv
Chapter 1	Introduction and Literature Survey	1-50
	1.1 g-C ₃ N ₄ : brief historical background and synthesis process	2-9
	1.2 Structural, Optical and Morphological features	
	1.2.1 Structural features of bulk g-C ₃ N ₄	10-12
	1.2.2 Optical features of g-C ₃ N ₄ and band gap	13
	1.2.3 Morphological features of g-C ₃ N ₄ and Dimensionality	14-15
	1.3 Carbon composites and g-C ₃ N ₄ as substitute of N doped carbon	16
	1.4 Potential application area of g-C ₃ N ₄ and its Composites	17-18
	1.4.1 Limitation of bulk g-C ₃ N ₄ for practical application	19
	1.4.2 Functionalization of g-C ₃ N ₄ : heterostructures/heterojunction	20
	1.4.3 Renewable energy and role of g-C ₃ N ₄ as an electrocatalyst	21
	1.4.3.1 Hydrogen (H ₂) as an energy carrier	22
	1.4.3.2 g-C ₃ N ₄ and its composites as HER electrocatalyst	23-24
	1.4.3.3 Figures of Merit for electrocatalyst	
	1.4.3.3 (a) Onset potential and over potential	
	1.4.3.3 (b) Exchange current density (<i>j₀</i>)	
	1.4.3.3 (c) Tafel equation and Tafel slope	
	1.4.3.3 (d) Gibbs free energy of adsorption and Volcano plot	25-32
	1.4.3.3 (e) Stability	
	1.4.3.3 (f) Faradic efficiency	
	1.4.3.3 (g) Turnover frequency (ToF)	
	1.4.3.4 Mechanism of HER	
	1.4.3.5 OER and its mechanism	
	1.4.3.6 Oxygen Reduction Reaction (ORR)	33
	1.4.4 Carbon nitride as the next generation of carbon-based supercapacitors	34-36
	1.4.4 (a) Role of different bonding state of nitrogen in catalytic activity	37

	<p>1.4.4 (b) Electrolyte selection in energy conversion and energy storage</p> <p>1.4.5 g-C₃N₄ as photocatalyst materials</p> <p>1.4.5.1 g-C₃N₄ for photocatalytic organic dye degradation</p> <p>1.4.5.1 (a) Z-scheme photocatalysis</p> <p>1.4.5.1 (b) Semiconductor heterojunctions: types</p> <p>1.4.5.1 (c) Ternary photocatalytic heterostructures</p> <p>1.4.5.2 g-C₃N₄ as sensing material</p> <p>1.4.5.2 (a) Fluorescent sensing by CNQDs</p> <p>1.4.5.2 (b) Lifetime of fluorescent material</p> <p>1.4.5.2 (c) Fluorescent quantum yield (QY)</p> <p>1.4.5.2 (d) Limit of detection (LOD)</p> <p>1.4.6 g-CN as catalyst support</p>	<p>38</p> <p>39-42</p> <p>43-47</p> <p>47</p>
	1.5 Scope of the work and objective of the thesis	48-50
Chapter 2	Characterization Techniques	51-73
	<p>2.1 Structural Characterization</p> <p>2.1.1 X-ray diffraction</p> <p>2.1.2 Raman Spectroscopy</p> <p>2.1.3 Fourier transform infrared spectroscopy</p> <p>2.1.4 UV visible spectroscopy</p> <p>2.1.5 Fluorescence spectroscopy</p>	<p>53</p> <p>54</p> <p>55-56</p> <p>57-58</p> <p>59</p>
	<p>2.2 Morphological Characterization</p> <p>2.2.1 Scanning electron microscopy (SEM) and Field-emission scanning electron microscopy (FE-SEM)</p> <p>2.2.1 (a) Secondary electron detector (SE2)</p> <p>2.2.1 (b) Secondary electron In-lens detector</p> <p>2.2.1 (c) Backscattered electron detector (AsB)</p> <p>2.2.1 (d) Backscattered electron In-lens detector (EsB)</p> <p>2.2.1 (e) An X-Ray dispersive energy detector</p> <p>2.2.2 Transmission electron microscopy (TEM) and high-resolution TEM (HR-TEM)</p>	<p>59-60</p> <p>61</p> <p>62-63</p>
	<p>2.3 Elemental analysis</p> <p>2.3.1 X-ray photoelectron spectroscopy (XPS)</p> <p>2.3.2 Energy dispersive x-ray analysis (EDX)</p>	<p>64</p> <p>65</p>
	2.4 Surface area analysis: Brunauer–Emmett–Teller (BET) Theory	66-67
	<p>2.5 Electrochemical workstation: CHI7044 and electrochemical methods</p> <p>2.5.1 Working electrode</p> <p>2.5.2 Reference electrode</p> <p>2.5.3 Counter (Auxiliary) electrode</p> <p>2.5.4 Cyclic voltammetry and linear sweep voltammetry</p> <p>2.5.5 Amperometry, chronoamperometry and</p>	68-73

	chronopotentiometry 2.5.6 Faradic and capacitive current	
Chapter 3	Ternary Nanocomposite of red P, reduced Graphene Oxide and graphitic Carbon Nitride (red P-rGO-g-C ₃ N ₄) as Metal-Free Electro-catalysts for Hydrogen Evolution Reaction	74-100
	3.1 Introduction	75-77
	3.2 Experimental Section 3.2.1 Materials 3.2.2 Synthesis of g-C ₃ N ₄ 3.2.3 Synthesis of Graphene Oxide (GO) 3.2.4 Synthesis of red P-rGO-g-C ₃ N ₄ composite 3.2.5 Preparation of composite ink and electrode modification 3.2.6 Instrumentations	78-81
	3.3 Results and discussion 3.3.1 Structural characterization of prepared ternary nanocomposites 3.3.2 Morphological Analysis 3.3.3 Elemental Analysis 3.3.4 Surface Area Analysis 3.3.5 Electrocatalytic HER study	82-99
	3.4 Concluding remarks	100
Chapter 4	Iron-Iron carbide (Fe/Fe ₃ C) encapsulated in S, N co-doped graphitic carbon as robust HER electrocatalyst	101-122
	4.1 Introduction	102-103
	4.2 Experimental Section 4.2.1 Materials 4.2.2 Synthesis of S, N co-doped iron/iron carbide 4.2.3 Instrumentations	104-106
	4.3 Results and discussion 4.3.1 Structural and morphological Study of as-prepared samples 4.3.2 Elemental Analysis 4.3.3 Raman Study and surface area analysis 4.3.4 Electrochemical measurements	107-120
	4.4 Conclusions	121-122
Chapter 5	Facile Synthesis of Doped C _x N _y QDs as Photoluminescent Matrix for Direct Detection of Hydroquinone	123-145
	5.1 Introduction	124-125
	5.2 Experimental Section 5.2.1 Materials 5.2.2 Synthesis of O-and S-doped C _x N _y QDs 5.2.3 Instrumentations	126-129
	5.3 Results and Discussion 5.3.1 Morphological and structural characterization 5.3.2 Elemental Analysis in the as-prepared C _x N _y QD 5.3.3 Optimization of PL activity	130-143

	<p>5.3.3.1 Excitation dependent PL intensity of QDs</p> <p>5.3.3.2 pH dependence of PL intensity of QDs</p> <p>5.3.3.3 Control experiment</p> <p>5.3.4 H₂Q detection by PL quenching</p> <p>5.3.4.1 H₂Q detection</p> <p>5.3.4.2 Selectivity of O- and S- doped C_xN_y QDs and real sample analysis</p> <p>5.3.4.3 Possible detection mechanism</p>	
	5.4 Conclusion	144-145
Chapter 6	Comparative study of enhanced photodegradation of azo dye by ternary nanocomposite Ag ₂ O/SnO ₂ @g-C ₃ N ₄ under natural and artificial light sources	146-183
	6.1 Introduction	147-149
	<p>6.2 Experimental Section</p> <p>6.2.1 Materials</p> <p>6.2.2 Synthesis of pure g-C₃N₄</p> <p>6.2.3 Synthesis of binary Ag₂O@g-C₃N₄ and SnO₂@g-C₃N₄ nanocomposites</p> <p>6.2.4 Synthesis of Ag₂O/SnO₂@g-C₃N₄ nanocomposite</p> <p>6.2.5 Characterization tools</p>	150-153
	<p>6.3 Results and discussion</p> <p>6.3.1 Structural analysis</p> <p>6.3.2 Elemental analysis of ternary composites</p> <p>6.3.3 Optical analysis</p> <p>6.3.4 Morphological analysis</p> <p>6.3.5 Photocatalytic degradation study under different light sources</p> <p>6.3.6 Scavenger test and stability of the ternary nanocomposite</p> <p>6.3.7 Degradation study of real samples discharged in industrial effluent</p> <p>6.3.8 Mechanism of dye degradation</p>	154-182
	6.4 Conclusion	183
Chapter 7	Conclusions	
	7.1 Summary	184-187
	7.2 Spaces for future work	
Appendix-A		188-198
Appendix-B	Morphology control synthesis of g-C ₃ N ₄ and doping with alkali metal ions for greater charge storage	199-212
	B.1 Introduction	199-201
	<p>B.2 Experimental Section</p> <p>B.2.1 Materials</p> <p>B.2.2 Synthesis of porous g-C₃N₄ (pCN)</p> <p>B.2.3 Synthesis of Alkali Metals Doped Porous g-C₃N₄</p> <p>B.2.4 Characterization Tools</p>	202-204

	B.3 Results and discussion	
	B.3.1 Characterization of porous g-C ₃ N ₄ (p-CN) and alkali metals doped porous g-C ₃ N ₄	205-211
	B.3.2 Electrochemical measurements	
	B.4 Conclusions	212
References		213-237
List of Publications		238-239
List of Conferences/Workshop/Symposium Attended		240-241

List of Figures

Figure No.	Figure Caption	Page Number
Figure 1.1	Heptazine (tri-s-triazine) and Melon ($C_6N_9H_3$) _n .	2
Figure 1.2	Triazine and tri-s-triazine (heptazine) based g- C_3N_4 . The circled part shows the repeating unit of the respective structures.	3
Figure 1.3	Various Precursors for the synthesis of g- C_3N_4 and reaction pathway for the synthesis of graphitic carbon nitride.	4
Figure 1.4	Two different reaction pathways for the synthesis of triazine based graphitic carbon nitride and tri-s-triazine based graphitic carbon nitride.	5
Figure 1.5	Proposed Tautomeric forms of melam.	6
Figure 1.6	Calculated energy diagram for the synthesis of carbon nitride.	7
Figure 1.7	The top-down and bottom-up synthesis strategies for carbon nitride nano sheets (CNNSs).	9
Figure 1.8	Same weight amount of g- C_3N_4 prepared from two different precursors.	11
Figure 1.9	XRD pattern of the polymeric carbon nitride, revealing a graphitic structure with 3.26 Å of an interplanar stacking distance of aromatic units and the distance from one nitride pore to another nitride pore (size of one tri-s-triazine unit).	12
Figure 1.10	Ultraviolet–visible diffuse reflectance spectrum of the polymeric carbon nitride. Inset is the g- C_3N_4 prepared at 550 °C in our lab and corresponding Tauc plot.	14
Figure 1.11	Different bonding states of nitrogen atoms into the carbon (graphene) atmosphere.	17
Figure 1.12	Schematic illustration of the applications domains of g- C_3N_4 based heterojunction/heterostructure.	18
Figure 1.13	Schematic illustration of the various functionalization techniques deployed for the carbon nitride for the task specific application.	20
Figure 1.14	Sustainable pathways from solar energy to Hydrogen (H_2).	21
Figure 1.15	A volcano plot of experimentally measured exchange current density as a function of the DFT-calculated Gibbs free energy of adsorbed atomic hydrogen.	29
Figure 1.16	The mechanism of hydrogen evolution on the surface of an electrode in acidic solutions.	31
Figure 1.17	The OER mechanism for acid (blue line) and alkaline (red line) conditions.	32
Figure 1.18	Direct Z-scheme photocatalysts.	41
Figure 1.19	Three kinds of semiconductor heterojunctions based on band alignment.	42
Figure 1.20	Jablonski Diagram for Fluorescence and Phosphorescence.	44

Figure 2.1	Diffraction pattern of X-ray into the sample and Photograph of the Diffractometer.	53
Figure 2.2	Rayleigh and Raman scattering by molecule upon irradiating with laser of wavelength λ .	54
Figure 2.3	Block-diagram and Photograph of FTIR Spectrophotometer.	56
Figure 2.4	Schematic diagram of the UV-visible spectrophotometer and Photograph of the Spectrophotometer.	57
Figure 2.5	Schematic diagram of the components of SEM microscope and Photograph of the SEM instruments.	60
Figure 2.6	Photograph of the FESEM instruments.	62
Figure 2.7	Schematic diagram of the components of TEM microscope and Photograph of the TEM instruments.	63
Figure 2.8	Photoelectron effect in XPS and Photograph of the XPS spectrophotometer.	65
Figure 2.9	Photograph of the Surface area measurement instrument.	66
Figure 2.10	Block Diagram of the CHI7044 instrument.	68
Figure 2.11	A representative electrochemical cell.	69
Figure 2.12	LSV waveform, CV waveform and Cyclic Voltammogram.	70
Figure 2.13	Variation of peak current in cyclic voltammogram as a function of scan rate.	71
Figure 3.1	Schematic diagram representing the synthesis of metal free ternary nano-composite P-rGO-g-C ₃ N ₄ .	80
Figure 3.2	XRD patterns of g-C ₃ N ₄ , rGO, rGO-g-C ₃ N ₄ , Red P, 10-20-30-40P-rGO-g-C ₃ N ₄ respectively and FT-IR spectrum of g-C ₃ N ₄ , rGO, rGO-g-C ₃ N ₄ , 10-20-30-40P-rGO-g-C ₃ N ₄ respectively.	83
Figure 3.3	FESEM images of g-C ₃ N ₄ , rGO, Red P, rGO-g-C ₃ N ₄ , 10P-rGO-g-C ₃ N ₄ , 20P-rGO-g-C ₃ N ₄ , 30P-rGO-g-C ₃ N ₄ and 40P-rGO-g-C ₃ N ₄ .	86
Figure 3.4	EDX Elemental mapping of 10P-rGO-g-C ₃ N ₄ , 20P-rGO-g-C ₃ N ₄ , 30P-rGO-g-C ₃ N ₄ and 40P-rGO-g-C ₃ N ₄ composites.	87
Figure 3.5	TEM images of g-C ₃ N ₄ , rGO-g-C ₃ N ₄ and 30P-rGO-g-C ₃ N ₄ respectively.	88
Figure 3.6	Deconvoluted XPS peaks of C1s, N1s, O1s, and P2p in 10P-rGO-g-C ₃ N ₄ , 20P-rGO-g-C ₃ N ₄ , and 30P-rGO-g-C ₃ N ₄ respectively.	89
Figure 3.7	Nitrogen adsorption desorption isotherm and corresponding pore volume distribution curves of g-C ₃ N ₄ , rGO-g-C ₃ N ₄ and 30P-rGO-g-C ₃ N ₄ respectively.	91
Figure 3.8	(A) Polarization curves of g-C ₃ N ₄ , rGO, rGO-g-C ₃ N ₄ , 30P-rGO-g-C ₃ N ₄ and 20% Pt/C in 0.5 M H ₂ SO ₄ at scan rate of 5 mV sec ⁻¹ (B) Polarization curves of 10/20/30/40P-rGO-g-C ₃ N ₄ along with 20% Pt/C (C) Tafel plots of g-C ₃ N ₄ , rGO-g-C ₃ N ₄ and 30P-rGO-g-C ₃ N ₄ , in inset 20% Pt/C (D) Tafel plots of 10/20/30/40P-rGO-g-C ₃ N ₄ (E) polarization curves of 30P-rGO-g-C ₃ N ₄ at different scan rates and (F) Polarization curves of 30P-rGO-g-C ₃ N ₄ initially, after 300 sweeps and after 500 sweeps at scan rate of 5 mV sec ⁻¹ .	93

Figure 3.9	Polarization curves of 30P-rGO-g-C ₃ N ₄ prepared by sonication method (physical mixing) and by hydrothermal treatment; and B. Polarization curve of 30P-rGO-g-C ₃ N ₄ in neutral, alkali and acidic media.	95
Figure 3.10	FESEM image of 30P-rGO-g-C ₃ N ₄ before (A) and after (B) performing CVs (300 and 500 sweeps).	96
Figure 3.11	A. Comparative cyclic voltammetry of g-C ₃ N ₄ , rGO-g-C ₃ N ₄ and 30P-rGO-g-C ₃ N ₄ at scan rate of 100 mV sec ⁻¹ ; B. CVs of 30P-rGO-g-C ₃ N ₄ at various scan rates; C. electrochemical double layer capacitance (C _{dl}) of g-C ₃ N ₄ , rGO-g-C ₃ N ₄ and 30P-rGO-g-C ₃ N ₄ and D. Stability test of 30P-rGO-g-C ₃ N ₄ modified Toray paper electrode at static over potential of -670 mV vs. Ag/AgCl for 2 h (7200 s) in 0.5 M H ₂ SO ₄ .	99
Figure 4.1	Synthesis protocol of doped carbon encapsulated iron-iron carbide (Fe/Fe ₃ C).	105
Figure 4.2	XRD spectra of iron carbide and its doped variants and zoomed-in XRD pattern of Fe@C-SN/25 from 2θ = 35 to 55° range.	107
Figure 4.3	SEM images of Fe@C, Fe@C-SN/25, Fe@C-SN/50 and Fe@C-SN/75.	108
Figure 4.4	SEM EDX spectra of the as-prepared samples.	109
Figure 4.5	TEM and HRTEM images of Fe@C-SN/50 along with SAED pattern.	110
Figure 4.6	High resolution deconvoluted Fe2p, C1s, N1s and S2p peaks of doped Fe@C-SN/25, Fe@C-SN/50 and Fe@C-SN/75 samples.	112
Figure 4.7	Raman spectrum of the synthesized samples.	114
Figure 4.8	N ₂ adsorption-desorption isotherm of equal HER performing catalysts; Fe@C-SN/50 and Fe@C-SN/25.	115
Figure 4.9	(a) LSV polarization curves (scan rate 5 mV/sec) of Fe@C along with its doped variants; (b) Corresponding Tafel slopes; (c) Calculation of double layer capacitance (C _{dl}) of doped variants of Fe@C; (d) CVs of doped variants at scan rate of 100 mV sec ⁻¹ ; (e) Stability LSVs of Fe@C-SN/25 and (f) Fe@C-SN/50 after multiple CV sweeps at scans rate of 5 mV/sec.	117
Figure 4.10	LSV polarization curves of (a) Fe@C-SN/25 and (b) Fe@C-SN/50 at various scan rates.	120
Figure 5.1	Schematic diagram for synthesis of O- and S-doped C _x N _y QDs. Inset shows aqueous dispersion of as-prepared C _x N _y QDs.	127
Figure 5.2	TEM image and the corresponding particle size distribution histogram of CM61.	130

Figure 5.3	FE-SEM image of as prepared C_xN_y QDs and adjacent EDS shows presence of all four elements O, S, C and N in the prepared quantum dots.	131
Figure 5.4	UV-vis absorbance (blue line) and PL spectra (red line); FT-IR spectrum, zeta potential curve and Tauc's plot of as-prepared CM61 QDs.	132
Figure 5.5	XPS survey spectrum and deconvoluted individual elemental peaks of as-prepared CM61 QD for C_{1s} , N_{1s} , O_{1s} and S_{2p} .	134
Figure 5.6	Emission spectra of CM61 at excitation wavelengths from 280 nm to 420 nm; plot of emission peak position corresponding to excitation wavelength; PL intensity of CM61 at various pHs and variation of PL intensity with pH value.	136
Figure 5.7	PL emission intensity of prepared sample under continuous irradiation of UV light (365nm).	137
Figure 5.8	PL emission spectrum of CM61 upon addition of various concentrations of H_2Q solution and relationship between $(F_0 - F)/F_0$ and concentration of H_2Q .	138
Figure 5.9	Selectivity of the CM61 for 8 μM H_2Q detection in presence of various interfering agents.	141
Figure 5.10	Plausible mechanism of H_2Q detection using CM61 QDs.	144
Figure 6.1	Synthesis protocol of ternary nanocomposite ($Ag_2O/SnO_2@g-C_3N_4$).	152
Figure 6.2	XRD pattern of $g-C_3N_4$, Ag_2O , SnO_2 , 33 % $SnO_2@g-C_3N_4$, 33 % $Ag_2O@g-C_3N_4$ and 33 % $Ag_2O/SnO_2@g-C_3N_4$ and FTIR spectra of bulk $g-C_3N_4$ and other composite materials.	155
Figure 6.3	XPS (A) survey analysis, (B) C_{1s} , (C) N_{1s} , (D) O_{1s} for 25% $Ag_2O/SnO_2@g-C_3N_4-11$ and comparative analysis of (E) Sn_{3d} and (F) Ag_{3d} for 25% $Ag_2O/SnO_2@g-C_3N_4-11$ with pure SnO_2 and Ag_2O respectively.	157
Figure 6.4	(A). UV-vis DRS spectra of (a) $g-C_3N_4$, (b) 33% $SnO_2@g-C_3N_4$, (c) 33% $Ag_2O@g-C_3N_4$ and (d) 33% $Ag_2O/SnO_2@g-C_3N_4$; (B). Plot of $(\alpha hv)^{1/2}$ vs hv for band gap energy of (a) $g-C_3N_4$ and $(\alpha hv)^2$ vs hv for bandgap energy of (b) Ag_2O and (c) SnO_2 ; and (C). Photoluminescence spectra (PL) of (a) $g-C_3N_4$, (b) 33% $Ag_2O@g-C_3N_4$, (c) 33% $SnO_2@g-C_3N_4$ and (d) 33% $Ag_2O/SnO_2@g-C_3N_4$ composites.	160
Figure 6.5	Time resolved PL decay spectra for the charge carrier in the $g-C_3N_4$ and 33% $Ag_2O/SnO_2@g-C_3N_4-11$.	162
Figure 6.6	TEM images of (a) 33% $Ag_2O@g-C_3N_4$, (b) 33% $SnO_2@g-C_3N_4$, (c) 33% $Ag_2O/SnO_2@g-C_3N_4$, (d) HRTEM image of 33% $Ag_2O/SnO_2@g-C_3N_4$, and corresponding (e) SAED pattern of 33% $Ag_2O/SnO_2@g-C_3N_4$.	163
Figure 6.7	TEM elemental mapping of 33% $Ag_2O/SnO_2@g-C_3N_4$ and corresponding EDX spectrum.	164
Figure 6.8	FE-SEM image of 25% $Ag_2O/SnO_2@g-C_3N_4$ along with elemental mapping and EDX spectrum.	165

Figure 6.9	N ₂ adsorption-desorption isotherm of nanocomposites and corresponding pore volume distribution plot.	167
Figure 6.10	A. Photocatalyst assisted degradation of Rh B over various composites; B. Absorption spectra of Rh B in presence of Ag ₂ O/SnO ₂ @g-C ₃ N ₄ composite under various sunlight irradiation times; C. First-order kinetic plots over various composites and D. comparison of rate constant values of (a) g-C ₃ N ₄ , (b) 25% SnO ₂ @g-C ₃ N ₄ , (c) 33% SnO ₂ @g-C ₃ N ₄ , (d) 25% Ag ₂ O@g-C ₃ N ₄ , (e) 33% Ag ₂ O@g-C ₃ N ₄ , (f) 33% Ag ₂ O/SnO ₂ @g-C ₃ N ₄ , and (g) 25% Ag ₂ O/SnO ₂ @g-C ₃ N ₄ -11.	169
Figure 6.11	Photocatalytic dye degradation under (A). sunlight exposure and (B). white LED light by different ratios of metal oxide loaded g-C ₃ N ₄ .	171
Figure 6.12	Rh B dye solution irradiation under sunlight in absence of photocatalyst.	171
Figure 6.13	A. Photocatalyst assisted degradation of Rh B over various composites under white light LED irradiation; B. Absorption spectra of Rh B in presence of 33% Ag ₂ O/SnO ₂ @g-C ₃ N ₄ composite; C. First-order kinetic plots over various composites and D. comparison of rate constant values of (a) g-C ₃ N ₄ , (b) 25% SnO ₂ @g-C ₃ N ₄ , (c) 25% Ag ₂ O@g-C ₃ N ₄ , (d) 33% SnO ₂ @g-C ₃ N ₄ , (e) 33% Ag ₂ O@g-C ₃ N ₄ , (f) 25% Ag ₂ O/SnO ₂ @g-C ₃ N ₄ , and (g) 33% Ag ₂ O/SnO ₂ @g-C ₃ N ₄ -11.	173
Figure 6.14	Comparison of dye degradation efficiency under two different light sources and their corresponding rate constant plot; (a and c denotes 33 % Ag ₂ O/SnO ₂ @g-C ₃ N ₄ -11; b and d denotes 25 % Ag ₂ O/SnO ₂ @g-C ₃ N ₄ -11).	175
Figure 6.15	(A) Rh B dye degradation in presence of (a) p-benzoquinone, (b) EDTA, (c) DMSO (c) methanol and (e) no scavengers; (B) reuse-recycle 2 nd and 3 rd run of 25% Ag ₂ O/SnO ₂ @g-C ₃ N ₄ composite.	176
Figure 6.16	(A) TOC evaluation and mineralization efficiency under sunlight and LED for 25% Ag ₂ O/SnO ₂ @g-C ₃ N ₄ and 33% Ag ₂ O/SnO ₂ @g-C ₃ N ₄ respectively and (B) UV-vis absorption spectra of industrial effluent before the exposure to the sunlight and after complete degradation of dye using 25% Ag ₂ O/SnO ₂ @g-C ₃ N ₄ -11.	178
Figure 6.17	Proposed plausible dye degradation mechanism over the prepared catalyst.	180
Figure A.1	XRD pattern and FTIR spectra of graphene oxide (GO) and reduced graphene oxide (rGO) after their individual hydrothermal treatment at 200°C for 16 hours.	189
Figure A.2	EDX spectrum of 10/20/30/40P-rGO-g-C ₃ N ₄ composites	189
Figure A.3	XPS survey spectrum of g-C ₃ N ₄ , rGO-g-C ₃ N ₄ , 10P-rGO-g-C ₃ N ₄ , 20P-rGO-g-C ₃ N ₄ and 30P-rGO-g-C ₃ N ₄ .	190
Figure A.4	Images of electrochemical set up for testing HER stability in 0.5M H ₂ SO ₄ .	190

Figure A.5	Full scan XPS survey spectrum of all doped species and undoped Fe@C.	191
Figure A.6	High resolution C1s and Fe2p XPS peaks of undoped Fe@C.	191
Figure A.7	UV-Visible absorption spectrum of H ₂ Q and emission spectrum of as-prepared CNQDs.	192
Figure A.8	Quenching of PL intensity of C _x N _y QDs by H ₂ Q in 7.4 pH phosphate buffer solution (PBS) and in N ₂ saturated PBS solution.	192
Figure A.9	Vibration spectra of (a) SnO ₂ and (b) Ag ₂ O nanoparticles.	193
Figure A.10	UV-visible DRS spectra of Ag ₂ O and SnO ₂ nanoparticles.	193
Figure A.11	XRD pattern of ternary composites 25% Ag ₂ O/SnO ₂ @g-C ₃ N ₄ before use and after 3 rd photocatalytic run.	194
Figure B.1	Schematic diagram of the synthesis of alkali metal-doped porous g-C ₃ N ₄ (pCN-3M).	203
Figure B.2	Photograph of the acid-treated melamine (dispersed in ethylene glycol) and the as-prepared alkali metal-doped porous g-C ₃ N ₄ .	205
Figure B.3	X-ray diffraction pattern of different alkali metal-doped porous g-C ₃ N ₄ (pCN) along with g-C ₃ N ₄ and X-ray diffraction pattern of 3/5/7 wt. % Li doped pCN materials.	206
Figure B.4	SEM images of (a) g-C ₃ N ₄ , (b) pCN, (c) pCN-3Li, (d) pCN-3Na and (e) pCN-3K.	207
Figure B.5	SEM images of (a) pCN-3Li, (b) pCN-5Li and (c) pCN-7Li	208
Figure B.6	(a) GCD curves of pCN, pCN-3Li, pCN-3Na and pCN-3K at current density of 0.2 A/g, (b) GCD curves of 3/5/7 wt. % Li added pCN at 0.1 A/g, (c) comparison plot of specific capacitance at 0.1, 0.2 and 0.5 A/g for g-C ₃ N ₄ , pCN, pCN-3Li, pCN-3Na and pCN-3K and (d) comparison plot of specific capacitance at 0.1, 0.2 and 0.5 A/g for 3/5/7 wt. % Li added pCN.	209
Figure B.7	GCD curves of pCN-3Li at current density 0.1, 0.2 and 0.5 A/g.	211
Figure B.8	Cyclic voltammograms of g-C ₃ N ₄ , pCN, pCN-3Li, pCN-3Na and pCN-3K and pCN and 3/5/7 wt. % Li doped pCN at a scan rate of 100 mV/sec.	212

List of Tables

Table No.	Table Caption	Page No.
Table 3.1	EDAX data for % atomic phosphorous present in different P-rGO-g-C ₃ N ₄ composites.	87
Table 4.1	Atomic % of elements present at the surface of the samples analyzed from XPS analysis.	113
Table 4.2	ECASA, Roughness factor (RF) and specific current density (J_s) at 0.45 V over potential (η) of all electrocatalysts.	119
Table 5.1	Quantum yields of C _x N _y QDs prepared by various molar ratios of precursors.	128
Table 5.2	A comparison of quantum yield of doped C _x N _y with others reported C-dots and carbon nitride dots.	129
Table 5.3	Comparison of different methods for detection of H ₂ Q.	140
Table 5.4	Determination of H ₂ Q in real samples.	142
Table 6.1	Binding states and peak positions of constituting elements of ternary nanocomposites.	158
Table 6.2	Specific surface area and average pore volume of the nanocomposites and g-C ₃ N ₄ .	167
Table 6.3	Rate constants of various catalysts dispersed in dye solution under irradiation from Sunlight and White light LED.	174
Table 6.4	Comparison of the photocatalytic performance of the as-proposed nanocomposite with earlier research works.	182
Table A.1	Correlative assignments of all the major vibrational peaks in individuals and composites.	195
Table A.2	Binding energy of various binding states of elements present in the as-prepared samples from XPS analysis.	196
Table A.3	Peak assignment of various peaks obtained along with area and FWHM values from Raman analysis.	197
Table A.4	Electrochemical analysis of doped and undoped Fe@C species.	198

List of Acronyms/Abbreviations

2D	:	Two dimensional
4NP	:	4-Nitrophenol
AC	:	Activated carbon
Aq.	:	Aqueous
BA	:	Benzoic acid
BET	:	Brunauer–Emmett–Teller
BJH	:	Barrett-Joyner-Halenda
CB	:	Conduction band
Cf.	:	Compare
CN	:	Carbon nitrides
CNNSs	:	Carbon nitride nanosheets
CNQDs	:	Carbon nitride quantum dots
CNT	:	Carbon nano tube
Conc.	:	Concentrated
CSs	:	Carbon-based supercapacitors
CT	:	Charge transfer
CV	:	Cyclic Voltammetry
CVD	:	Chemical vapor deposition
C_{dl}	:	Double-layer capacitance
C_{sp}	:	Specific capacitance
ECASA	:	Electrochemically active surface area
EDX/EDS	:	Energy-dispersive X-ray spectroscopy
EIS	:	Electrochemical impedance spectroscopy

Eq.	:	Equation
FCEVs	:	Fuel cell electric vehicle
FE	:	Faradic efficiency
FESEM	:	Field emission scanning electron microscopy
FTIR	:	Fourier transform infrared spectroscopy
FWHM	:	Full width at half maxima
GC	:	Glassy carbon
GCD	:	Galvanic Charge Discharge
GO	:	Graphene oxide
H.	:	Hours
H ₂ Q	:	Hydroquinone
HER	:	Hydrogen evolution reaction
HRTEM	:	High resolution transmission electron microscopy
ICSD	:	Inorganic crystal structure data
ICP-MS	:	Inductively coupled plasma-mass spectrometry
IUPAC	:	International Union of Pure and Applied Chemistry
IR	:	Infra-Red
LCPDS	:	Joint Committee on Powder Diffraction Standards
LED	:	Light emitting diode
LOD	:	Limit of detection
LSV	:	Linear Sweep Voltammetry
MOF	:	Metal organic framework
MOR	:	Methanol oxidation reaction
NC	:	N-doped carbon

nm	:	Nano-molar
NPs	:	Nanoparticles
OCP	:	Open circuit potential
OER	:	Oxygen evolution reaction
ORR	:	Oxygen reduction reaction
pCN	:	Porous g-C ₃ N ₄
PBS	:	Phosphate buffer solution
PEMFCs	:	Proton exchange membrane fuel cells
PL	:	Photoluminescence
QDs	:	Quantum dots
QY	:	Quantum Yield
RDE	:	Rotating disk electrode
rGO	:	Reduced graphene oxide
Ref.	:	Reference
R.F.	:	Roughness factor
Rh B	:	Rhodamine B
RHE	:	Reversible hydrogen electrode
SAED	:	Selected area electron diffraction
SEM	:	Scanning electron microscopy
SI	:	Supporting information
SHE	:	Standard hydrogen electrode
STP	:	Standard temperature and pressure
Temp.	:	Temperature
TEM	:	Transmission electron microscopy

THF	:	Tetrahydro furan
TMDCs	:	Transition metal dichalcogenides
TOC	:	Total organic carbon
UHV	:	Ultra High Vacuum
UV-DRS	:	UV-diffuse reflectance spectroscopy
UV-vis	:	UV-visible
VB	:	Valence band
VLMs	:	Visible-light microscopes
Wt.	:	Weight
XPS	:	X-ray photoelectron spectroscopy
XRD	:	X-ray diffraction
μm	:	Micro-molar

Preface

Energy conservation and environmental protection have remained an issue of great attention among scientific communities and climate activists from past decades. It has also stimulated the greater utilization of solar energy and renewables to bridge the gap between energy demand and energy consumption. Research efforts in the twenty-first century are directed more towards finding effective alternatives of fossil-based fuels in form of clean and renewable energy. At the same time, harnessing the solar power to drive the related reaction is of great significance to protect the Mother Nature from hazardous materials by their sensitive detection and selective remediation. Such necessities also come under the ambit of the sustainable development goals (SDGs) 6, 7, 13 and 14 set up by the United Nations General Assembly in 2015.

Deployment of H₂ as an energy carrier into fuel cells has acted as a promising milestone as it has a high energy density (120–142 MJ kg⁻¹). Hydrogen generation by electrocatalytic water splitting driven by renewable electricity is a promising pathway for the sustainable hydrogen economy as it also leads to less consumption of fossil-based fuels which in turn controls climate change. Noble metal platinum is still the best electrocatalyst for this purpose with a high exchange current density (j_0) and small Tafel slope, but its higher cost acts as a hindrance for commercial use. The research community is looking for an alternative of this precious metal, in this effort, transition metal-based carbide and carbon composites as an electrocatalyst and earth-abundant non-metal element-based materials viz. g-C₃N₄ are of great interest. Besides fossil-based fuels which emit greenhouse gas on combustion, there are many industrial pollutants and chemicals of carcinogenic nature such as azo dyes and phenolic compounds which are listed by the US

Environmental Protection Agency under the hazardous category for the environment. The sensitive detection and cost-effective removal of these anti-nature materials are part of the wide agenda of policy-making bodies at the global level.

The graphitic carbon nitride (g-C₃N₄) has drawn wide research interest owing to being a metal-free catalyst, easy to synthesize, stable to a range of acid-alkaline solution and its non-toxicity. The g-C₃N₄ is one of the oldest synthetic polymers having an N-rich framework and semiconductor features with a band gap value of 2.7 eV. It is visualized as a substitute for N-doped carbon composites.

The focus of the present thesis is to explore the electrocatalytic and photochemical features of the g-C₃N₄ and other carbon-based composites to address the energy issues and better environmental protection. We have focused our efforts on the functionalization of g-C₃N₄ with others semiconductor metal oxides, non-metal elements as well as carbon species that yield enhanced results via synergism.

The complete thesis work is divided into the seven chapters. The *Chapter 1* details about the graphitic carbon nitride, its history and synthesis process, dimensionality of g-C₃N₄ viz. zero-dimension, one dimension, two dimension and three-dimension, application areas of this 2D material and its limitation in bulk form. This chapter also talks about the various parameters of HER catalysts, charge storage features, photocatalytic features of g-C₃N₄ with other semiconducting metal oxide composites and appearance of fluorescent properties at zero dimension of carbon nitride viz. quantum dots. The *Chapter 2* covers concise details about the tools and instruments utilized for the characterization purpose of the as-synthesized samples as well as electrochemical instruments and related terminology. The *Chapter 3* explores the HER properties of nanocomposites prepared using various

weight % of red P immobilized over the rGO-g-C₃N₄ binary structure hydrothermally. This study sheds light on the exploration of earth-abundant metal-free element-based catalysts as an alternate for noble metal Pt. The **Chapter 4** is about the further exploration of transition metal-based carbides for the electrocatalytic HER properties by doping of heteroatoms Sulphur and nitrogen into the graphitic carbon encapsulation. The obtained results are significant in highlighting the role of heteroatoms for enhancing the active sites resulting in greater activity by the catalyst. The **Chapter 5** details the fluorescent sensing features of zero dimension of carbon nitride i.e., quantum dots. The S and O doped surface of carbon nitride quantum dots do detection of pollutant hydroquinone (H₂Q) by photoluminescence quenching via surface electron transfer. The **Chapter 6** again explores the photochemical properties of metal oxide-carbon nitride nanocomposites by photocatalytic dye degradation phenomenon. The optimal combination of semiconducting metal oxides Ag₂O and SnO₂ over the surface of g-C₃N₄ proves the most effective for the degradation of common textile azo dye under the sunlight as well as white light LED. The **Chapter 7** summarizes the complete research works and also highlights the space available to explore further viz. future scope in the work done so far.

The present thesis has compiled all the published results in *Electrochimica Acta* (2020 IF: 6.901), *ACS Energy & Fuels* (2020 IF: 3.605), *Spectrochimica Acta Part A* (2020 IF: 4.098), and *Materials Chemistry and Physics* (2020 IF: 4.094). ‘**Appendix B**’ covers the exploratory work of charge storage properties of g-C₃N₄ by structural modification and alkali metal doping at interlayers of g-C₃N₄.